Title

A Theoretical Model for Computing Freezing Point Depression of Lithium-Ion Battery Electrolytes

Journal

Journal of The Electrochemical Society, 168(12)

ISSN

0013-4651

Authors

Self, Julian
Bergstrom, Helen K
Fong, Kara D
et al.

Publication Date

2021-12-01

DOI

10.1149/1945-7111/ac3e47

Peer reviewed

Journal of The Electrochemical Society

OPEN ACCESS

A Theoretical Model for Computing Freezing Point Depression of Lithium-Ion Battery Electrolytes

To cite this article: Julian Self *et al* 2021 *J. Electrochem. Soc.* **168** 120532

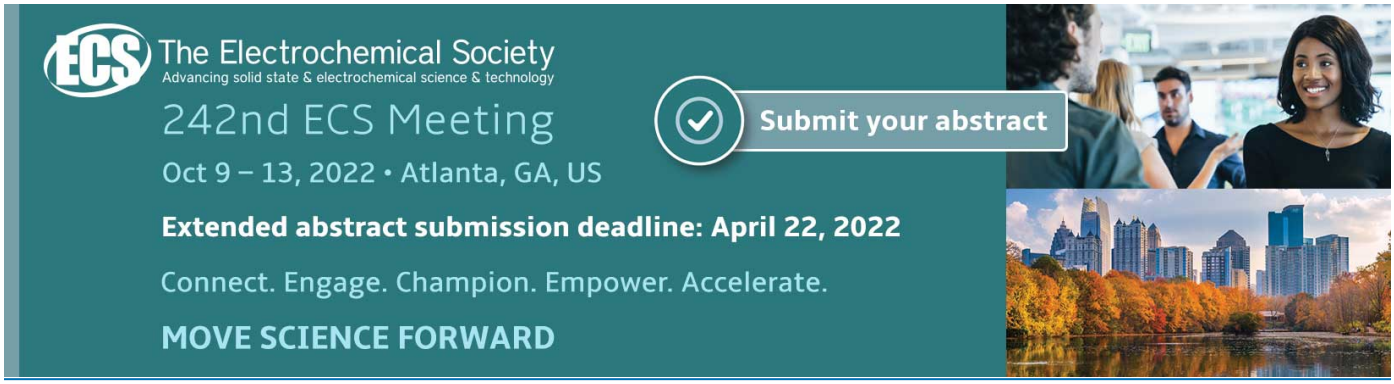

Journal of The Electrochemical Society, 2021 **168** 120532

A Theoretical Model for Computing Freezing Point Depression of Lithium-Ion Battery Electrolytes

Julian Self,[1,2] Helen K. Bergstrom,[2,3] Kara D. Fong,[2,3] Bryan D. McCloskey,[2,3] and Kristin A. Persson[1,2,4,z]

[1]*Department of Materials Science and Engineering, University of California, Berkeley, United States of America*
[2]*Energy Technologies Area, Lawrence Berkeley National Laboratory, United States of America*
[3]*Department of Chemical and Biomolecular Engineering, University of California, Berkeley, United States of America*
[4]*The Molecular Foundry, Lawrence Berkeley National Laboratory, United States of America*

Reliable prediction of freezing point depression in liquid electrolytes will accelerate the development of improved Li-ion batteries which can operate in low temperature environments. In this work we establish a computational methodology to calculate activity coefficients and liquidus lines for battery-relevant liquid electrolytes. Electronic structure methods are used in conjuction with classical molecular dynamics simulations and theoretical expressions for Born solvation energy, ion-atmosphere effects from Debye-Hückel theory and solvent entropic effects. The framework uses no a priori knowledge beyond neat solvent properties and the concentration of salt. $LiPF_6$ in propylene carbonate (PC), $LiPF_6$ in dimethyl carbonate (DMC) and $LiClO_4$ in DMC are investigated up to 1 molal with accuracy better than 3 °C when compared to experimental freezing point measurements. We find that the difference in freezing point depression between the propylene carbonate-based electrolyte and the dimethyl carbonate electrolytes originates from the difference in the solvent dielectric constant.
 [DOI: 10.1149/1945-7111/ac3e47]

Manuscript submitted September 13, 2021; revised manuscript received October 22, 2021. Published December 22, 2021.

Supplementary material for this article is available online

The importance of phase equilibria for lithium ion battery (LIB) electrolytes is well known.[1–12] Phase behavior, as described by phase diagrams, helps determine the operating windows of liquid electrolytes. Recently, there is a significant effort devoted to extending the viability of LIB to lower temperatures (T),[13,14] and as such knowledge of the exact freezing point of liquid electrolytes is pertinent. Moreover, the freezing point depression is directly related to fundamental thermodynamics and the physical chemistry of liquid electrolytes through the activity coefficients, which affect electrochemical stability and transport behavior. In this work we develop a methodology to obtain the freezing point depression and activity coefficients of LIB-relevant electrolytes from computational methods for concentrations up to 1 molal (m). We undertake case studies for three systems of interest: $LiPF_6$ in propylene carbonate (PC), $LiClO_4$ in dimethyl carbonate (DMC), and $LiPF_6$ in DMC. These systems are chosen as the two solvents are significantly different in nature (low vs high permittivity and linear vs cyclic) and there is significant thermodynamic data already published to compare our results to.

Kinetics of charge transfer as well as bulk transport in electrodes and in electrolytes are a concern at low temperature.[15–17] In this work we specifically focus on challenges associated with bulk transport in the electrolyte at low temperatures. In order to maintain sufficient conductivity, it is essential that the electrolyte of use remains in liquid phase, i.e., does not freeze[17]—motivating this work. If we consider the low temperature range necessary for deployment of LIBs in cold climates from −40 °C to 25 °C, then conventionally-used ternary electrolytes[11] are inadequate as they generally show freezing at ∼−20 °C.[1,17,18] Freezing point depression, θ, is the difference in the freezing point of the neat solvent and that of the electrolyte. In a binary, single-solvent electrolyte θ can be computed from the solvent activity a_{solvent}, knowing neat solvent properties such as the freezing temperature T_0, the enthalpy of fusion $\Delta\overline{H}_{\text{fus}}$ and the difference in heat capacity between the two phases Δc_P, with the gas constant denoted as R:[19]

$$\theta = \frac{\Delta\overline{H}_{\text{fus}} - 2RT_0 \ln a_{\text{solvent}} - \sqrt{2\Delta c_P T_0^2 R \ln a_{\text{solvent}} + \Delta\overline{H}_{\text{fus}}^2}}{2\Delta\overline{H}_{\text{fus}}/T_0 + \Delta c_P - 2R \ln a_{\text{solvent}}}. \quad [1]$$

In the above equation, $\Delta\overline{H}_{\text{fus}}$ and Δc_P are assumed constant as a function of temperature.

Herein, we first discuss theoretical schemes to compute salt activity coefficients, which are directly related to the solvent activity, a_{solvent}.[20] Ideal solutions, Debye-Hückel theory,[20–22] Pitzer-type models,[23–27] and the mean spherical approximation[28,29] (MSA), are discussed. We then propose an alternative approach, which involves Debye-Hückel theory augmented with Born solvation,[30–32] ion pairing[29] and solvent entropic effects related to the free solvent fraction.[33] We present methodology to obtain the ionic radii[34] and concentration-dependent dielectric constant,[35] which are input parameters used in our proposed theoretical approach. The obtained thermodynamic properties, used in conjunction with neat solvent properties, allow calculation of liquidus lines in the phase diagrams which are compared to experimental measurements.

Salt Activity Coefficients

Various models may be used to compute the molal salt activity coefficient, $\gamma_{\pm}$, which, for 1-1 electrolytes, appears in the expression for the chemical potential of the salt in solution (denoted μ_{salt}, with the infinite dilution salt reference state denoted as μ^0_{salt}) as follows:

$$\mu_{\text{salt}} - \mu^0_{\text{salt}} = 2RT \ln(\gamma_{\pm} m) \quad [2]$$

In the simplest case, we can assume ideality ($\gamma_{\pm} = 1$), implying there are no interactions between species in solution. In this case, Eq. 2 simplifies to the following:

$$\mu_{\text{salt}} - \mu^0_{\text{salt}} = 2RT \ln(m) \quad [3]$$

The Debye-Hükel (DH) theory of electrolyte solutions considers the change in the chemical potential of an ion in solution due to the ionic environment,[20,22] where the molality of positive and negative ions are written as m_- and m_+:

[z]E-mail: kapersson@lbl.gov

$$\mu_{salt} - \mu^0_{salt} = RT\ln(\gamma_{DH,+}) + RT\ln(\gamma_{DH,-}) + RT\ln(m_+) + RT\ln(m_-) \quad [4]$$

DH theory accounts for ion-ion interactions via a mean field approach where the Poisson-Boltzmann equation is linearized.[20,22] When used alone, DH theory assumes full dissociation of ions. An analytic DH solution exists, and the DH activity coefficient $\gamma_{DH,i}$ can be explicitly written as follows, with z_i as species charge:[20,34]

$$\ln\gamma_{DH,i} = -z_i^2\frac{A_{DH}\sqrt{I}}{1 + B_{DH}\alpha_{DH}\sqrt{I}} \quad [5]$$

DH theory predicts a decrease of $\gamma_{DH,i}$ with increasing ionic strength (i.e., as we add salt). The molal ionic strength, I, is defined via the following expression:

$$I = 0.5\sum_i z_i^2 m_i \quad [6]$$

The DH term B_{DH} is defined by the following expression, where F is Faraday's constant, ε_0 is the electric constant, ε is the permittivity, and ρ_0 the neat solvent density:

$$B_{DH} = \frac{F}{(\varepsilon_0\varepsilon RT/2)^{0.5}}\sqrt{\rho_0} \quad [7]$$

α_{DH} is the distance of closest approach between ions,[34] e.g., the sum of radii of cation and anion species. The DH parameter A_{DH} can be expressed via the following relationship, where the units are the square root of inverse molality, allowing A_{DH} to often be expressed as unitless provided the ionic strength is also in units of molality. An expression for A_{DH} is as follows, where e is the elementary charge:

$$A_{DH} = \frac{Fe}{8\pi\varepsilon_0\varepsilon RT}B_{DH} \quad [8]$$

At sufficiently high concentrations (e.g., above 0.01 m), DH theory alone is insufficient to account for all non-idealities due to, among many factors, changes in permittivity, changes in specific ion-ion and ion-solvent interactions (e.g., ion pairing).[22,36] Empirically, this can be accounted for via a Guggenheim-type equation:[20,37,38]

$$\ln\gamma_{Gugg,i} = \ln\gamma_{DH,i} + B_K I + C_K I^{3/2} \quad [9]$$

However, the exact physical origins of B_K and C_K are unspecified and as such these coefficients cannot be calculated a priori. Similar to the Guggenheim-type expression, the Pitzer equations are widely used semi-empirical expressions for the activity of aqueous and non-aqueous electrolytes.[24–27] The equations are as follows:

$$\ln(\gamma_\pm) = \frac{-A^\phi\sqrt{I}}{1 + b\sqrt{I}} - \frac{2A^\phi}{b}\ln(1 + b\sqrt{I}) + mB^\gamma + \frac{3}{2}m^2C^\phi \quad [10]$$

$$B^\gamma = 2\beta^{(0)} + \xi^{(1)} + \xi^{(2)} \quad [11]$$

$$\xi^{(i)} = \frac{2\beta^{(i)}}{\alpha_i^2 I}\left[1 - \left(1 + \alpha_i\sqrt{I} - \frac{1}{2}\alpha_i^2 I\right)\exp(-\alpha_i\sqrt{I})\right] \quad [12]$$

$$A^\phi = \frac{A_{DH}}{3} \quad [13]$$

Seven parameters must be adjusted: b, $\beta^{(0)}$, $\beta^{(1)}$, $\beta^{(2)}$, α_1, α_2 and C^ϕ. Generally, all seven of these parameters cannot be predicted a priori. Moreover, often in calculating the ionic strength, it is assumed that there is no ion pairing and the concentration of charged species is the same as the concentration of the salt.[26,27] Especially in low permittivity media, this assumption is incorrect and the Pitzer-type model is implicitly fit to experimental data via unreasonably large ionic radii. For example, we can identify b with $B_{DH}\alpha_{DH}$ where $B_{DH} = 16.52\ \text{nm}^{-1}$ and b has been reported as 95 for DMC-based electrolytes,[26,27] implying $\alpha_{DH} = 5.75$ nm. This value is unreasonably large and the parameter b is arguably used to mask the shortcomings of the Pitzer-type model at accounting for long-range electrostatics. This is discussed further below. A theoretical alternative to the Guggenheim-type and Pitzer-type models is the MSA,[28,29,39–42] which builds on DH-theory in that the ions' radii now contribute to an additional volume exclusion term to the chemical potential. However, MSA by itself does not account for the effects of the concentration-dependent change in permittivity of electrolytes, which is known to be important especially in low permittivity electrolytes.[43] Some scholarship has allowed for MSA enhanced with consideration of concentration-dependent permittivity effects,[44,45] although with many adjustable parameters, which may not be obtainable a priori. Thus, since the MSA either uses many adjustable parameters or does not account for concentration-dependent permittivity effects, it is herein avoided. Moreover, the work presented here is suggested as an alternative to theories with adjustable parameters, while both capturing the important underlying physical chemistry in solution and predicting thermodynamics properties with reasonable accuracy.

Theory

In this work we propose to account for non-idealities with consideration of Born solvation, ion pairing effects and free solvent number, in addition to DH theory. This departs from Pitzer and MSA models which, when applied alone, ignore Born solvation and free solvent effects. DH theory accounts for long-range ion-ion interactions between all charged species. Born solvation accounts for long-range ion-solvent interactions via the dielectric medium of the electrolyte created by the solvent molecules and polar associated salt species (e.g., ion pairs). Ion pairing[29] accounts for specific, short-range, ion-ion interactions. Ion pairs are formed when closely interacting ions form a single kinetic entity, i.e., move together for an appreciable amount of time.[29] These may be unimportant in certain aqueous electrolytes due to the high dielectric constant of the aqueous solvent, but ion pairing generally becomes more important as the polarity of the solvent decreases. For example, in low permittivity solvents ($\varepsilon < 10$), ion pairing may be significant even in the semi-dilute regime.[29,43] The simplest 1-1 electrolyte ion pairing equilibrium involves species, S, of free ions S_+, S_- and contact-ion pairs (CIP), S_{CIP}:

$$S_+ + S_- \rightleftharpoons S_{CIP} \quad [14]$$

In lithium-salt carbonate-solvent electrolytes, the solvent and cation interact very strongly, such that the cation and its full solvation shell form long-lived clusters.[46] Thus, in this work, cations are considered with their primary solvation shell, which is assumed to hold a fixed number of solvent molecules. Moreover, we will account for the entropic losses that result upon free solvent binding to cations, as well as the entropic gains from solvent molecules released upon ion pairing. If a cation, via its primary solvation shell, is bound to $n_{s,+}$ solvent molecules S_0 and the CIP to $n_{s,CIP}$ solvent molecules, the ion-pairing equilibrium can be written as follows:

$$((S_0)_{n_{s,+}}S_+) + S_- \rightleftharpoons ((S_0)_{n_{s,CIP}}S_{CIP}) + (n_{s,+} - n_{s,CIP})S_0 \quad [15]$$

For the above equilibrium, we can denote the infinite dilution association constant $K_A^0 = \exp(-\Delta G_A^0/RT)$, where G_A^0 is the free energy change upon ion pairing, as in Eq. 15. We note that there may be equilibria with higher order associated species and aggregates,[29] which are not considered in this work but would likely be necessary for investigations of concentrations above 1 m in Li-ion electrolytes.

For a fraction of free ions α, we can establish the following:

$$\mu_{\text{salt}} - \mu^0_{\text{salt}} = \alpha\mu_+ + \alpha\mu_- + (1-\alpha)\mu_{\text{CIP}} \quad [16]$$

We can write the expression for the individual contributions to the chemical potential of free ions as the following, where $\gamma_{B,i}$ refers to the Born solvation contribution to the activity coefficient, and $\gamma_{FSL,i}$ the entropic contribution from free solvent loss:

$$\mu_+ - \mu^0_+ = RT\ln(\gamma_{DH,+}) + RT\ln(\gamma_{B,+}) + RT\ln(\gamma_{FSL,+}) + RT\ln(m_+) \quad [17]$$

Similarly, for the anion, we can write:

$$\mu_- - \mu^0_- = RT\ln(\gamma_{DH,-}) + RT\ln(\gamma_{B,-}) + RT\ln(m_-) \quad [18]$$

Explicitly, the Born solvation expression[31,32] is:

$$\ln(\gamma_{B,i}) = \frac{e^2}{8\pi\varepsilon_0 R_{B,i}RT}\left(\frac{1}{\varepsilon(m)} - \frac{1}{\varepsilon(m=0)}\right) \quad [19]$$

In the above equation $R_{B,i}$ is the Born radius. Accordingly, for an ion of a fixed radius $R_{B,i}$, its free energy is lowered if the medium it is dissolved in incurs an increase in dielectric constant. The third term on the right-hand side of Eq. 17 is relevant to the entropy loss of free solvent molecules from formation of cation solvation shells. For a species which binds solvent molecules (e.g., cations or CIPs), the chemical potential contribution from the loss in free solvent entropy from the creation of the solvation shell can be written as:[47]

$$\ln(\gamma_{FSL,i}) = -n_{s,i}\ln\left(\frac{m_{\text{free solvent}}}{m_{\text{solvent}}}\right) \quad [20]$$

where $m_{\text{free solvent}}$ is the molality of free solvent, which, at infinite dilution, is equal to the neat solvent molality ($m^0_{\text{free solvent}} = m_{\text{solvent}}$, see Supplemental Information for further details stacks.iop.org/JES/168/120532/mmedia). In this work it is assumed anions do not bind solvent molecules (vide infra). The free solvent molality can be calculated knowing the concentration of species and the solvation numbers $n_{s,+}$ and $n_{s,CIP}$:

$$m_{\text{free solvent}} = m_{\text{solvent}} - m_+ n_{s,+} - m_{\text{CIP}} n_{s,\text{CIP}} \quad [21]$$

In Eq. 16 the chemical potential of the CIP μ_{CIP} is:

$$\mu_{\text{CIP}} = -RT\ln(K^0_A) + RT\ln(\gamma_{FSL,\text{CIP}}) + RT\ln(m_{\text{CIP}}) \quad [22]$$

The first term accounts for the fact that the reference state is that of free ions at infinite dilution, where all free ion and CIP activity coefficients are set to $\gamma_i = 1$.

α, which appears in Eq. 16, is related to the concentration equilibrium constant K_A, defined via the following mass action law:[29]

$$K_A = \frac{m_{\text{CIP}}}{m_+ m_-} = \frac{1-\alpha}{\alpha^2 m} \quad [23]$$

We can also relate the concentration equilibrium constant K_A to K^0_A via:[29]

$$K_A = K^0_A \frac{\gamma_{DH,+}\,\gamma_{B,+}\,\gamma_{FSL,+}\,\gamma_{DH,-}\,\gamma_{B,-}}{\gamma_{FSL,\text{CIP}}} \quad [24]$$

Accordingly, K^0_A is concentration independent and is related to the concentration equilibrium constant via the relevant activity coefficients.[29]

A combination of Eqs. 16, 17, 18 and 22 provides an expression for the chemical potential as a function of the fraction of species and the various activity coefficients:

$$\mu_{\text{salt}} - \mu^0_{\text{salt}} = RT\left(\frac{m_+}{m}\ln(\gamma_{B,+}\,\gamma_{DH,+}\,\gamma_{FSL,+}\,m_+) + \frac{m_-}{m}\ln(\gamma_{B,-}\,\gamma_{DH,-}\,m_-) + \frac{m_{\text{CIP}}}{m}\ln\left(\frac{\gamma_{FSL,\text{CIP}} m_{\text{CIP}}}{K^0_A}\right)\right) \quad [25]$$

The quantity of interest, the experimentally accessible $\gamma_\pm$, is directly related to the chemical potential of the salt via arrangement

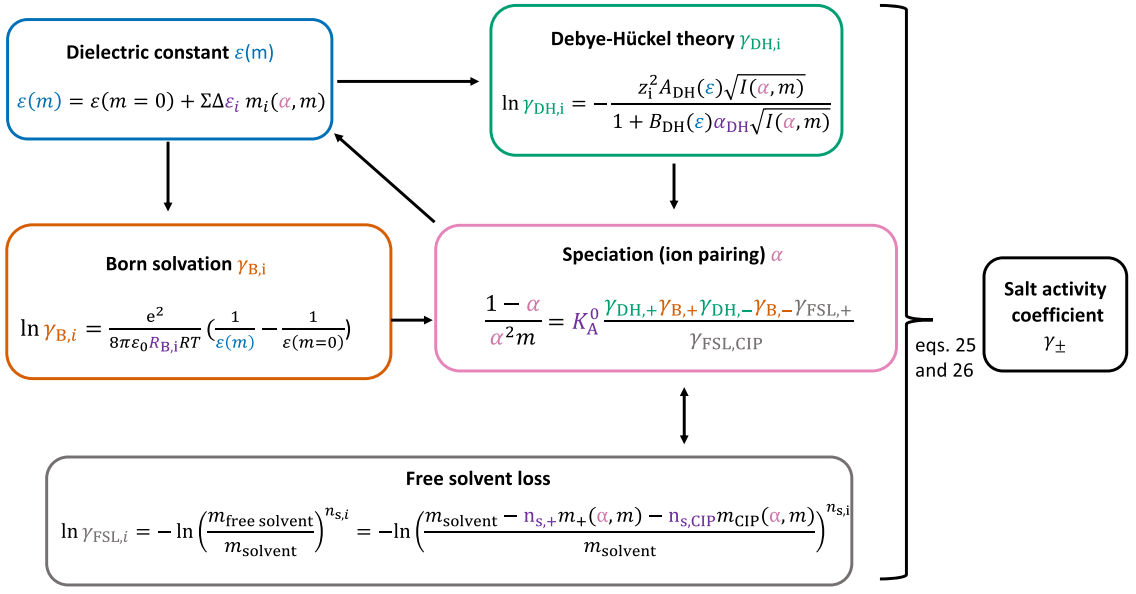

Figure 1. Schematic on methodology to compute the salt activity coefficient in the present work. Input parameters which are computed a priori and are not dependent on molality are shown in purple. We note $\alpha_{DH} = R_{B,+} + R_{B,-}$. The various theories employed (DH, Born solvation and ion pairing) are interdependent, as shown by arrows, and are also interdependent with the dielectric constant. Various quantities of interest are color-coded for visual ease. We further note $\alpha = \frac{m_+}{m} = \frac{m_-}{m} = \frac{m - m_{\text{CIP}}}{m}$.

of Eq. 2:

$$\gamma_{\pm} = \frac{1}{m}\exp\left(\frac{\mu_{salt} - \mu^{0}_{salt}}{2RT}\right) \quad [26]$$

Figure 1 shows a schematic on the methodology to compute the salt activity coefficient $\gamma_{\pm}$ in the present work. The parameters that are not dependent on molality and that are computed via electronic structure methods or molecular dynamics simulations are shown in purple. In the scheme proposed in this work, $\gamma_{\pm}$ can be calculated via Eqs. 5, 19, 20, 23, 25 and 26, and with knowledge of K^0_A, $\varepsilon(m)$, the values of $n_{s,i}$, $R_{B,i}$ and $\alpha_{DH,i}$. Since these latter quantities will be computed using either electronic structure or classical molecular dynamics methods, with no a priori experimental knowledge of the physical effects of salt on the electrolyte, we distinguish the herein used methodology from Pitzer-type models, which use adjustable parameters. Although the liquid electrolytes concepts of DH theory, Born solvation, ion pairing and free solvent number are well-known, to the authors' knowledge they have not been previously used together to obtain the chemical potential of species in a computational context. Presumably this is due to the difficulties of obtaining the concentration-dependent dielectric constant of the electrolyte.

Input parameters to model.—The radii of ions $R_{B,i}$ and ionic distance of closest approach α_{DH}, as appearing in Eqs. 5 and 19, are parameters that are used in the Born solvation theory and DH theory, respectively. In this work the DH distance α_{DH} is picked as the sum of the two relevant Born radii:

$$\alpha_{DH} = (R_{B,+} + R_{B,-}) \quad [27]$$

There are many approaches that can be used to obtain radii, either α_{DH} and/or $R_{B,i}$, for example, the experimental ionic radii (e.g., from solid salt crystals),[34,48] the experimental molar conductivity as a function of molar salt concentration $\Lambda(c)$,[43] the experimental activity coefficient $\gamma_{\pm}(m)$,[27,39] the experimental solvation energy $\Delta G^s_i(\varepsilon)$[49] and the computed solvation energy $\Delta G^s_i(\varepsilon)$.

Various radii are shown in Table I. There is no exact measure of radii in both DH theory and the Born theory of solvation.[34] Generally, it is accepted that the relevant measure of radii in solution should be somewhere between the "bare" ionic radii and the size of a solvated ion-cluster.[22] As expected, the crystallographic ("bare") ionic radii[50] shown in Table I are the smallest. For $LiClO_4$ and $LiAsF_6$ in DMC, the Born radii fit to molar conductivity (i.e., the conductivity normalized by salt concentration), $\Lambda(c)$, data have been reported. For these reported values, DH effects were neglected ($\gamma_{DH,i} = 1$) and, $R_{B,i}$ and K^0_A were simultaneously fit with the $\Lambda(c)$ data.[43] We show the reported values for AsF^-_6 as they are likely representative to those of PF^-_6 due to similar chemical structure and formula. Here, due to the investigators' inherent inability to decouple the activity coefficients of the anion and cation from fitting $\Lambda(c)$, the ions' radii are in effect equal. For the present work, we desire a methodology to obtain radii which does not require a priori experimental data, precluding for example the use of molar conductivity-obtained ionic radii. Here, the radii $R_{B,i}$ are solved for via the calculation of a change in the free energy of solvation ΔG^s_i, using the following equation:[49]

$$\Delta G^s_i(m \to 0) = \frac{e^2}{8\pi\varepsilon_0 R_{B,i}}\left(\frac{1}{\varepsilon_2(m=0)} - \frac{1}{\varepsilon(m=0)}\right) \quad [28]$$

Here, ΔG^s_i calculates the free energy change of a species solvated in solution as the dielectric constant changes from ε to ε_2. For Li^+ in DMC, $R_{B,Li} = 0.40$ nm was found via use of Eq. 28 and electronic structure methods. For cations, the first solvation shell was included in the electronic structure calculations, in addition to a continuum solvation model[51] (further details in Computational Methods). The value obtained for Li^+ in DMC is about five times larger than the "bare" ionic radii but closer to the experimental value fit from $\Lambda(c)$ data. The anions's radii were calculated in a similar fashion, in this case without an explicit first solvation shell as anion-solvent short range interactions are approximated here as negligible.[42,52] We note that preferential solvation of cations over anions is an active research topic.[53] As expected, the values for PF^-_6 found were very close to the "bare" ionic radii. For the PC electrolyte system, the computed PF^-_6 anion radius was identical as for the DMC system (0.31 nm). For Li^+, the radius value is smaller for the PC system (0.16 nm vs 0.40 nm for the DMC case). Although no analogous literature values for Born radii were found for Li^+ and PF^-_6 in PC, a previous publication reported a value of 1.5 Å for Li^+ in water,[49] which holds a comparable dielectric constant to PC. As discussed previously, using a Pitzer-model approach, the ionic radii obtained for DMC electrolytes are unreasonably overestimated, where the radii are those which are implicitly used in the DH term of the Pitzer-type equations ($R_{B,Li} \sim \alpha_{DH,Li}/2$). For example, the values for the Li^+-in-DMC radii with a Pitzer-type model are an order of magnitude larger than the size of the solvation shell,[26,27] and two orders of magnitude larger than the Li^+ crystallographic radius.

Table I. Radii and solvation number of ionic species obtained via various methods. PW refers to values computed and used in the present work.

	Radius	Notes	References
R_{Li}	0.076 nm	crystallographic radius	50
R_{PF6}	0.254 nm	crystallographic radius	50
R_{ClO4}	0.236 nm	crystallographic radius	50
$R_{B,Li}$(PC)	0.16 nm	from ΔG^s (Comp.)	PW
$R_{B,Li}$(DMC)	0.40 nm	from ΔG^s (Comp.)	PW
$R_{B,PF6}$(DMC)	0.31 nm	from ΔG^s (Comp.)	PW
$R_{B,PF6}$(PC)	0.31 nm	from ΔG^s (Comp.)	PW
$R_{B,ClO4}$(DMC)	0.30 nm	from ΔG^s (Comp.)	PW
$R_{B,Li}$(DMC), $R_{B,AsF6}$ (DMC)	0.63 nm	fit: Born, no DH from Λ(c)	43
$R_{B,Li}$(DMC), $R_{B,ClO4}$ (DMC)	0.58 nm	fit: Born, no DH from Λ(c)	43
$R_{B,Li}$(DMC), $R_{B,ClO4}$ (DMC)	3 nm	fit: Pitzer $\gamma_{\pm}$(m)	26
$R_{B,Li}$(DMC), $R_{B,PF6}$ (DMC)	3 nm	fit: Pitzer $\gamma_{\pm}$(m)	27
	Solvation Number		
$n_{s,+}$ (Li^+ in PC)	6	from MD	PW
$n_{s,CIP}$ ($LiPF_6$ in PC)	5	from MD	PW
$n_{s,+}$ (Li^+ in DMC)	5	from MD	PW
$n_{s,CIP}$ ($LiPF_6$ in DMC)	4	from MD	PW
$n_{s,CIP}$ ($LiClO_4$in DMC)	4	from MD	PW

Moreover, this is likely due to overfitting of the model—and more precisely, the lack of Born solvation (i.e., concentration-dependent permittivity effects) in the Pitzer model. This suggests that the use of the Pitzer-type equations to fit thermodynamic data of non-aqueous electrolytes may be more analogous to polynomial fitting than to a rigorous underlying theory. The computed solvation numbers ($n_{s,i}$ values between 4 and 6), listed in Table I, are in general agreement with previous reports.[46,54–59] Sample solvation structures obtained from MD are shown in Fig. S1.

In the current work, the concentration dependent dielectric constant, which is needed to compute Eqs. 5 and 19, requires knowledge of the speciation (e.g., the molality of each species m_i) and dielectric increment per species $\Delta\varepsilon_i$ and is calculated via the following:

$$\varepsilon(m) = \varepsilon(m = 0) + \Sigma\Delta\varepsilon_i m_i \qquad [29]$$

K_A^0, the $\Delta\varepsilon_i$ values, the $n_{s,i}$ values, the $R_{B,i}$ values, Eqs. 5, 19, 20, 24, 27, 29 and the neat solvent dielectric constant (Table II) were here used to simultaneously solve for speciation (m_i values) and $\varepsilon(m)$. The equations used form a system of non-linear coupled equations, in addition to the relationships for mass conservation and electroneutrality. Figure 1 shows the equations used in this methodology. A numerical approach to solve the non-linear coupled equations was developed with in-house code, available at https://github.com/JSelf42/FreezingPointDepression. Table III shows the values of K_A^0 computed and used in this work, as well as the computed dielectric increment values. K_A^0 values were computed from the above-described electronic structure calculations used for calculating the species' radii. Dielectric increment values were computed via classical molecular dynamic simulations (see Methods for further details). For the DMC systems, the computed K_A^0 values are higher than experimental ones. We encourage caution in comparing against experimental results as the experimental K_A^0 was obtained by simultaneously fitting the Born radii,[43] in this case neglecting DH effects. From equations (vide infra) 30 and 32, $\Delta\varepsilon_{CIP}$ is found to be considerably large and positive, reflecting the dipolar nature of CIP species. Similarly, $\Delta\varepsilon_i$ for free ions in DMC were found to slightly exceed zero, suggesting structure promotion. For the PC system, the computed K_A^0 is in excellent agreement with the reported experimental value. The cation $\Delta\varepsilon_i$ was found to be substantially negative (−44/m), which we attribute to the loss of free solvent molecules when PC molecules are bound in solvation shells (e.g., by the cation). Here, the positive CIP $\Delta\varepsilon_i$ reflects the significant dipole moment of the CIP. Once the speciation and dielectric constant are found as a function of concentration, Eqs. 25 and 26 allow to solve for the (experimentally accessible) $\gamma_\pm$, which is directly related to the solvent activity via the Gibbs-Duhem relation.[20] The calculated solvent activities $a_{solvent}$, as well as reported neat solvent properties which are shown in Table II, allow the calculation of the liquidus lines. The neat solvent properties used are the melting temperature, T_0, the enthalpy of fusion $\Delta\overline{H}_{fus}$, the change in heat capacity upon freezing Δc_P and the neat solvent density.[1,2] The relationships to obtain the liquidus from the solvent activity follow Ge and Wang,[19] as shown in Eq. 1.

In this work the activity coefficients are calculated at 25 °C, which allows comparison to reported data. The assumption that follows is that the activity coefficients calculated at room temperature can be used to reasonably estimate the activity coefficients near the freezing temperature of the liquid electrolyte. Considering the temperature dependence of activity coefficients is left to further work.

Computational methods.—*Association Constants, Radii and Solvation Numbers.*—Infinite dilution association constants K_A^0, shown in Table III, were calculated via first-principles quantum chemistry methods of the free energy change relevant to Eq. 15. More specifically, hybrid DFT calculations were undertaken with Gaussian 16[62] software using the wb97x-d functional with the 6-31 +g(d,p) basis set and a continuum solvation model (CSM)[51,63–65] using the neat solvent permittivity as well as an explicit solvation shell for cations (both free and in CIPs). Before geometry optimization via electronic structure methods, initial configurations were picked via conformational analysis using Macromodel and an OPLS-based force field, where structures with solvation numbers matching those from the classical MD simulations were picked. The latter were computed via analysis of the radial distribution function of species simulated via MD (vide infra). In order to correct for spurious contributions of low-frequency modes to the vibrational partition function for the electronic structure calculations, Truhlar's[66] correction was applied using the "GoodVibes" code package.[67] To obtain the Born radii of cations or anions, the continuum solvation model (i.e., PCM) dielectric constant was varied in the above-described calculations for free energy of species in solution, and the resulting energy change allowed calculation of the Born radius according to Eq. 28.

Dielectric increments.—Dielectric increment $\Delta\varepsilon_i$ calculations were done with classical molecular dynamics simulations, as discussed in previous publications.[64,68,69] For a total dipole moment $\mathbf{p}$ of the electrolyte system (which includes the contribution from associated salt species if present), ε of the electrolyte can be calculated as follows (neglecting electronic polarizability):

$$\varepsilon = 1 + \frac{\langle \mathbf{p}^2 \rangle - \langle \mathbf{p} \rangle^2}{3k_B TV\varepsilon_0} \qquad [30]$$

where V is the volume of the electrolyte.

The dipole moment is calculated by summing over the charge q_i of atoms i multiplied by their position $\mathbf{r_i}$:

$$\mathbf{p} = \Sigma q_i \mathbf{r_i} \qquad [31]$$

Single salt species (free ions or CIPs) were placed in a box (approximately 0.1 M) with solvent molecules (127 DMC molecules or 122 PC molecules) using PACKMOL.[70] With the GROMACS[71] MD software, these electrolytes were equilibrated first using a Berendsen barostat (NPT).[72] Afterwards, production runs in the NVT ensemble using the velocity rescaling thermostat were undertaken.[73] At least 2 production runs were undertaken per system. CIPs were associated for the duration of the simulation (each at least 10 ns) and from their dipole moment, in addition to the dipole moment of the solvent species, the dielectric constant of the entire electrolyte solution was found. The dielectric constant of the neat solvent solution was subtracted from this value, which was then subsequently divided by the concentration (e.g., 0.1 m) to obtain the

Table II. Experimental neat solvent properties used in this work. Bold values were measured in the present work.

Solvent	T_0 (°C)	$\Delta\overline{H}_{fus}$ (kJ/mol)	Δc_P (J/(mol K))	density (kg/L)	$\varepsilon(c = 0)$	References
PC	−48.8	8.960	33	1.20	65	1 2 60 61
DMC	**4.3**	**12.36**	29	1.07	3.1	1 2 43

Table III. Association constants and dielectric increment per salt species.

System	K_A^0 (1/M) PW	K_A^0 (1/M, exp) Refs. 43 50	$\Delta\varepsilon_{CIP}$ (1/m) PW	$\Delta\varepsilon_+$(1/m) PW	$\Delta\varepsilon_-$(1/m) PW
DMC/$LiPF_6$	3.5×10^{16}	8.9×10^{11}a)	23	2.9	1.2
DMC/$LiClO_4$	1.8×10^{17}	8.6×10^{12}a)	17	2.9	1.2
PC/$LiPF_6$	2.0	2.1	11	−44	−22

a) The thermodynamic assumptions used in fitting for this value from experiment[43] were significantly different than those used in the present work (see text).

dielectric increment per salt species, as appearing in Table III:

$$\Delta\varepsilon_i = \frac{\varepsilon(m_i) - \varepsilon(m=0)}{m_i} \quad [32]$$

For PC, the CIP was constrained using a Li-P(F_6) distance of 3.8 Å, the value obtained via electronic structure calculation. The partial charge assignments for the DMC molecule were taken from Soetens et al.,[74] while for PC they were generated using Macromodel software.[75] The latter were then subsequently scaled by 1.07 for the neat solvent dielectric constant to match that of experiment. The other parameters for the PC and DMC molecules are taken from the standard OPLS forcefield.[76,77] The parameter files for ClO_4^- and PF_6^- were taken from Doherty et al.[78] and Lopes et al.[79] The Li^+, of a charge of +1, followed the standard OPLS parameters.[76,77]

DSC Measurements

Battery grade lithium hexafluorophosphate ($LiPF_6$) and DMC were purchased from Gotion Inc. and directly transferred under inert atmosphere to an argon glove box (Vacuum Atmospheres) maintained below 5 ppm water and oxygen. Battery grade PC was purchased from Sigma Alrdrich. Electrolyte samples were prepared inside the glove box on a moles per kg solvent basis. Differential scanning calorimetry (DSC) measurements of DMC-based electrolytes were performed on a TA Instruments Q1000 DSC equipped with an RCS90 cooling system. 10 μL of electrolyte were hermetically sealed inside DSC pans (TA Instruments T-zero aluminum hermetic pans) inside the glove box. The DSC was calibrated prior to measurements using an indium metal standard (Sigma Aldrich). Samples were cycled between −40° and 30 °C at a ramp rate of 5 °C per minute. Each sample was subjected to an initial controlled heat-cool cycle to erase any thermal history prior to the heat cycle from which phase data was extracted. The liquidus was determined as the peak temperature in the melting endotherm during the second heating cycle. Three replicates were run for each electrolyte concentration. For PC-based electrolyte systems, DSC measurements were performed on a Perkin-Elmer DSC-8000 with a liquid-nitrogen cooling system and helium purge gas. The instrument was calibrated using indium and decane standards. 10 μl of electrolyte were hermetically sealed inside DSC pans (Perkin-Elmer aluminum hermetic pans) inside the glove box along with ∼1 mg of mesocarbon microbeads (MCMB) purchased from MTI Corporation. MCMBs were added in order to provide a nucleation site to reduce supercooling.[80] PC electrolytes were cycled between 0° and −100 °C at a ramp rate of 0.5 °C/min, with an isothermal hold at −100 °C for 12 h prior to reheating. Using this method a liquidus was measured for pure PC which was in good agreement with the literature. However no endothermic phenomena indicating melting was observed for $LiPF_6$ containing electrolytes with concentrations as low as 0.1 m.

Results

Figure 2 (top left) shows the calculated speciation diagram. We note that $m_+ = m_-$ and $m_{CIP} = m - m_+$ due to charge neutrality and mass conservation. $\varepsilon(m)$ is shown as a function of concentration (bottom left). For the DMC-based electrolytes, $\varepsilon(m)$ increases with m, due to the significant CIP fraction and large $\Delta\varepsilon_{CIP}$. In contrast, for the PC-based electrolytes, $\varepsilon(m)$ decreases due to the significant fraction of free ions and very negative cation $\Delta\varepsilon_i$. The trends in speciation and dielectric constant are consistent: the increase in dielectric constant of the low permittivity solvent systems leads to the trend of increase in free ion fraction (DMC systems), a phenomenon known as redissociation.[6,81] This increase in free ion fraction for the DMC-based systems is consistent with the reported molar conductivity increase with increasing concentration.[43,82,83] For the PC-based system, the decrease in dielectric constant with concentration, in addition to the mass action law, promotes a larger fraction of CIPs with increasing salt molality. The computed $\varepsilon(m)$ is larger than that from experiment above ∼0.5 m, which suggests in this regime the fraction of CIPs is overestimated, and free ion fraction underestimated. We speculate that the moderate disagreement of computed and experimental $\varepsilon(m)$ is due to an overestimation of K_A^0 and/or the neglect of more complex solvation effects, such as the concentration dependence of $n_{s,i}$.

Figure 2 (top right) shows $\gamma_\pm$ computed using Eqs. 25 and 26. For DMC-based electrolytes, $\gamma_\pm$ generally decreases with concentration as both the DH and Born effects reduce $\gamma_\pm$ more so than the free solvent loss increases $\gamma_\pm$ (Fig. S2). The computed values are shifted by an arbitrary constant value for comparison against experiment in the relevant concentration range, as thermodynamic values are only a function of the derivative of the logarithm of the activity coefficient, and not the absolute values. For the PC-based electrolyte, although the DH effects contribute to a lowering of $\gamma_\pm$, the permittivity decrease leads to an increase in $\gamma_\pm$ due to the Born solvation contribution of the ions. This distinction in behavior for high permittivity (e.g., PC-based) vs low permittivity electrolytes (e.g., DMC-based) also leads to the significant change in the activity of the solvent, shown in the bottom right of Fig. 2. The activity of the solvent was directly calculated from the computed $\gamma_\pm$.[20]

For comparison, Fig. S3 shows the logarithm of the salt activity coefficients when computed from DH-theory alone[34] using crystallographic radii.[50] Here, the neglect of ion pairing, permittivity effects and free solvent number changes and the use of crystallographic radii leads to incorrect activity coefficients. DH-theory alone predicts a monotonic decrease of activity coefficient with salt concentration. It cannot qualitatively predict that the activity coefficient of $LiPF_6$ salt in PC should increase and severely overestimates the decrease in $\gamma_\pm$ with concentration for DMC based electrolytes. This illustrates that DH theory, when used alone, is inadequate to model activity coefficients beyond the dilute limit.

Figure 3 shows the phase diagrams of the various studied electrolytes near the liquidus region from 0 to 1 m. In the top left, $LiPF_6$ in DMC is shown. The values were calculated following the freezing point depression calculated from Eq. 1. In the case of ideality, the activity of solvent can be computed assuming an osmotic coefficient of 1.[20] When compared to the ideal (theoretical) solution, the measured and computed liquidus lines are elevated to higher temperatures. This is due to the relatively high activity of the solvent in the DMC electrolyte, as shown in Fig. 2. In the bottom left, the phase diagram near the liquidus for $LiClO_4$ in DMC is shown. The result is analogous to $LiPF_6$ in DMC, since both ion pairing and long-range electrostatic interactions are comparable for both systems, given the similarity of the salt. In both DMC-based

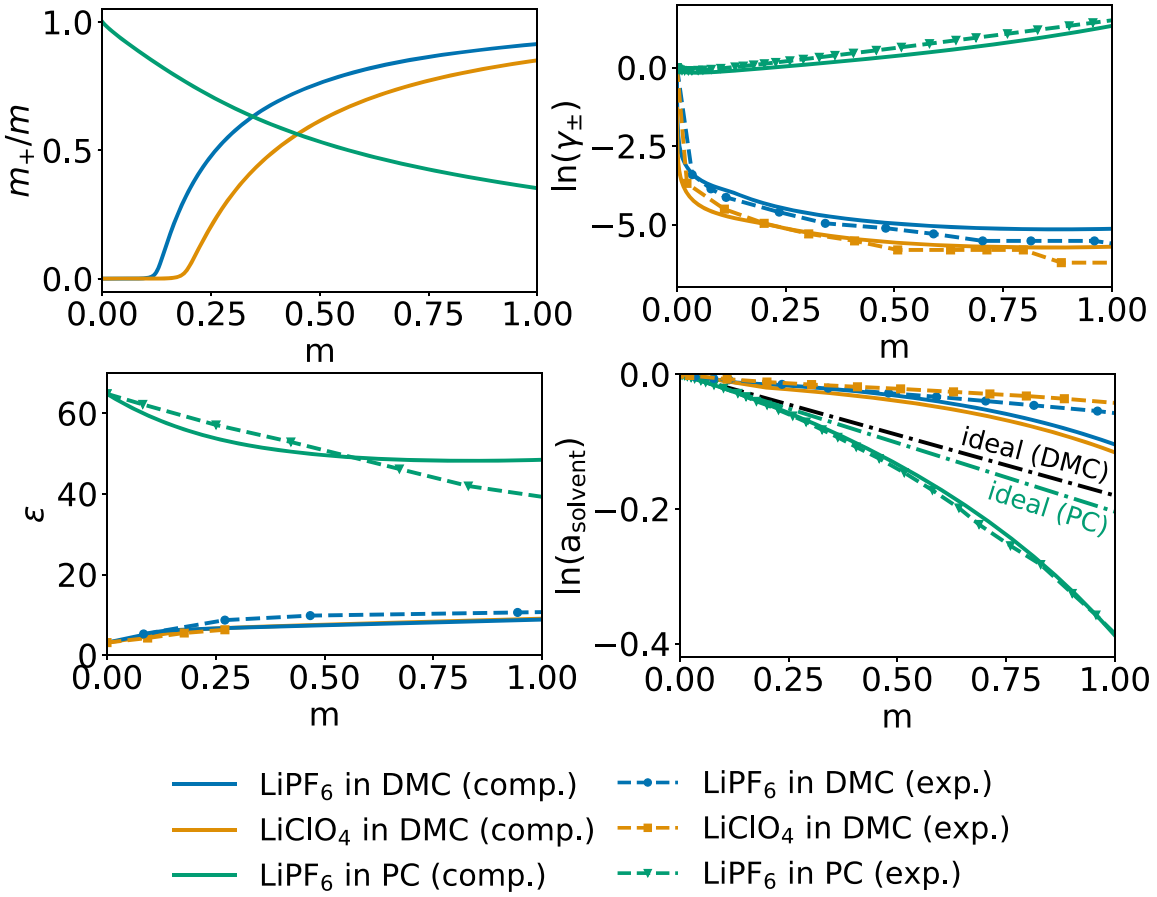

Figure 2. Speciation diagram for different electrolytes (top left). Dielectric constant ε as a function of concentration (bottom left). Logarithm of activity coefficient $\gamma_\pm$ as a function of concentration (top right), shifted by a constant arbitrary value (see text). Logarithm of solvent activity (bottom right). For the bottom left plot, computed data for $LiPF_6$ in DMC overlaps with that of $LiClO_4$ data. Experimental values are taken from literature.[26,27,43,60,82,84]

electrolyte cases, the agreement with experiment is excellent. Furthermore, the phase behavior from DSC data agrees with the computed and experimental $\gamma_\pm$ data and shows that the assumptions[19] in deriving Eq. 1 are reasonable. Moreover, for the $LiPF_6$ in DMC case, the measured liquidus line is in agreement with previous experimental reports.[9] We speculate that the slight disagreement of the computed liquidus line with experiment is due to the neglect of higher order associated salt species beyond CIPs.[43] Higher order aggregates such as neutral salt dimers have been proposed as non-polar,[43] and as such their presence would not be apparent from the measured $\varepsilon(m)$ alone (Fig. 2 bottom left). Nonetheless, the agreement between computed and measured $\gamma_\pm$ suggests that in this concentration range, consideration of such species may not be needed to accurately model phase behavior.

For $LiPF_6$ in PC, shown in the bottom right, the behavior vis-a-vis ideality is the opposite: the liquidus lines calculated from experimental and computed activity coefficient data show solution freezing at a lower temperature than that predicted for an ideal solution. This results from the lower solvent activity of the real solution with respect to an ideal solution, as shown in Fig. 2. The freezing point depression agreement between liquidus lines calculated from experimental and computed activity coefficient data is once again good. While direct observation of the liquidus of pure PC is possible, direct liquidus line measurements via DSC have proven unsuccessful due to the glass forming nature of PC-based electrolytes.[85,86] We hypothesize that the nucleation and crystallization are inhibited due to kinetic limitations and that, despite the lack of DSC data, the liquidus line computed from activity coefficient data is theoretically correct, within the assumptions herein. These assumptions include the neglect of the activity coefficient temperature dependence and that the studied concentration range (e.g., below 1 m) is lower than the eutectic composition. Furthermore, we note that the liquidus line in glassy systems such as $LiPF_6$ in PC provides a temperature bound above which there is necessarily a strictly liquid phase. In addition, we also note that the function relating solvent activity to freezing point depression (Eq. 1) is a function also of the freezing point of the neat solvent. Between various solvents of interest, this can lead to a freezing point depression change on the order of 5 °C. For example, the freezing point depression of an ideal DMC-based electrolyte would decrease by 3 °C at 1 molal if the DMC T_0 was that of PC.

In all cases the enthalpies of fusion and relevant heat capacities used in calculating the liquidus line were measured or found in existing literature (see Table II). Interestingly, for DMC and PC, these values are comparable, explaining why the ideal (theoretical) liquidus lines show comparable slopes. The results suggest that, provided similar enthalpies of fusion and heat capacities (liquid and solid) of the solvent, high permittivity electrolytes will generally show much greater freezing point depression than low permittivity electrolytes. These findings are expected to play a significant role in the future design of low-temperature LIB electrolytes. Further work on freezing point depression of electrolytes should include the study of different salts in addition to the treatment of ternary electrolytes (e.g., two co-solvents), which are more widely used than binary electrolytes for LIB applications.

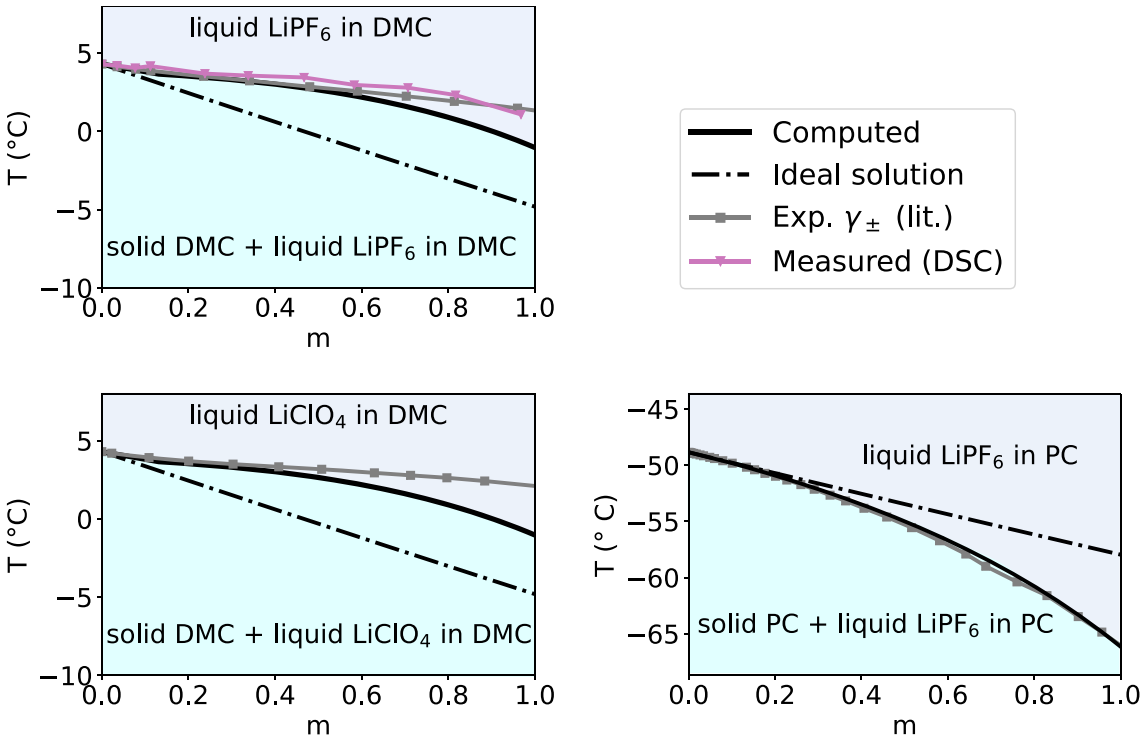

Figure 3. Phase diagrams near the liquidus line for $LiPF_6$ in DMC (top left), $LiClO_4$ in DMC (bottom left) and $LiPF_6$ in PC (bottom right). DSC measurements were carried by the authors, while experimental activity coefficient data used in the calculation of liquidus lines (gray) were taken from literature.[26,27,84]

Conclusions

In this work a theoretical model to compute activity coefficients and liquidus lines of phase diagrams was elaborated. Within the model, all parameters are computed via density-functional theory electronic structure and classical molecular dynamics simulations. The results were validated on three carbonate electrolytes, relevant to lithium-ion batteries, showing good to excellent agreement with experiment. Furthermore, beyond the predictive power of the methodology, our work elucidates how human-interpretable physicochemical properties such as ions' radii, ions' solvation number, the concentration-dependent dielectric constant and ion pairing affect the activity coefficients of liquid electrolytes. Finally, we find that high permittivity electrolytes generally show greater freezing point depression than linear carbonate based electrolytes since the former show a dielectric constant decrease with concentration and the latter show a dielectric constant increase with concentration.

Acknowledgments

DSC work at the Molecular Foundry was supported by the Office of Science, Office of Basic Energy Sciences, of the U.S. Department of Energy under Contract No. DE-AC02-05CH11231. We acknowledge support by the Assistant Secretary for Energy Efficiency and Renewable Energy, Vehicle Technologies Office, of the U.S. Department of Energy under Contract DE-AC02-05CH11231, under the Advanced Battery Materials Research (BMR) Program managed by Tien Duong as well as the Low Temperature Electrolyte Program. This research used resources of the National Energy Research Scientific Computing Center (NERSC), under Contract No. DE-AC02-05CH11231. We also acknowledge computational resources supported under NIH S10OD023532. H.K.B. further acknowledges support from NSF GRFP under Grant no. DGE 1 752 814. K.D.F is supported by the Berkeley Fellowship for Graduate Study.

ORCID

Julian Self https://orcid.org/0000-0002-5486-9559
Helen K. Bergstrom https://orcid.org/0000-0002-1209-6113
Kara D. Fong https://orcid.org/0000-0002-0711-097X
Bryan D. McCloskey https://orcid.org/0000-0001-6599-2336
Kristin A. Persson https://orcid.org/0000-0003-2495-5509

References

1. M. S. Ding, K. Xu, and T. R. Jow, "Liquid-Solid Phase Diagrams of Binary Carbonates for Lithium Batteries." *J. Electrochem. Soc.*, **147**, 1688 (2000).
2. M. S. Ding, "Liquid-Solid Phase Diagrams of Ternary and Quaternary Organic Carbonates." *J. Electrochem. Soc.*, **151**, A731 (2004).
3. M. S. Ding, "Liquid-Solid Phase Equilibria and Thermodynamic Modeling for Binary Organic Carbonates." *J. Chem. Eng. Data*, **49**, 276 (2004).
4. M. Ding, K. Xu, and T. Jow, "Phase Diagram of EC-DMC Binary System and Enthalpic Determination of its Eutectic Composition." *J. Therm. Anal. Calorim.*, **62**, 177 (2000).
5. M. S. Ding, "Thermodynamic Analysis of Phase Diagrams of Binary Carbonates Based on a Regular Solution Model." *J. Electrochem. Soc.*, **149**, A1063 (2002).
6. E. R. Logan, E. M. Tonita, K. L. Gering, L. Ma, M. K. G. Bauer, J. Li, L. Y. Beaulieu, and J. R. Dahn, "A Study of the Transport Properties of Ethylene Carbonate-Free Li Electrolytes." *J. Electrochem. Soc.*, **165**, A705 (2018).
7. R. Petibon, J. Xia, L. Ma, M. K. G. Bauer, K. J. Nelson, and J. R. Dahn, "Electrolyte System for High Voltage Li-Ion Cells." *J. Electrochem. Soc.*, **163**, A2571 (2016).
8. M. S. Ding, "Excess Gibbs Energy of Mixing for Organic Carbonates from Fitting of Their Binary Phase Diagrams with Nonideal Solution Models." *J. Solution Chem.*, **34**, 343 (2005).
9. D. J. Xiong, M. Bauer, L. D. Ellis, T. Hynes, S. Hyatt, D. S. Hall, and J. R. Dahn, "Some Physical Properties of Ethylene Carbonate-Free Electrolytes." *J. Electrochem. Soc.*, **165**, A126 (2018).
10. R. P. Day, J. Xia, R. Petibon, J. Rucska, H. Wang, A. T. B. Wright, and J. R. Dahn, "Differential Thermal Analysis of Li-Ion Cells as an Effective Probe of Liquid Electrolyte Evolution during Aging." *J. Electrochem. Soc.*, **162**, A2577 (2015).
11. K. Xu, "Nonaqueous Liquid Electrolytes for Lithium-Based Rechargeable Batteries." *Chem. Rev.*, **104**, 4303 (2004).
12. K. Xu, "Electrolytes and Interphases in Li-Ion Batteries and Beyond." *Chem. Rev.*, **114**, 11503 (2014).
13. R. Jow, S. S. Zhang, K. Xu, and J. Allen, "Electrolytes for Low Temperature Operations of Li-Ion Batteries." *ECS Trans.*, **3**, 51 (2007).

14. S. Tan, Z. Shadike, E. Hu, Q.-C. Wang, and X.-Q. Yang, "Propylene Carbonate-Based Electrolyte for Low Temperature Lithium Batteries." *ECS Meeting Abstracts* (2020).
15. S. Zhang, K. Xu, and T. Jow, "The Low Temperature Performance of Li-ion Batteries." *J. Power Sources*, **115**, 137 (2003).
16. A. J. Ringsby, K. D. Fong, J. Self, H. K. Bergstrom, B. D. McCloskey, and K. A. Persson, "Transport Phenomena in Low Temperature Lithium-Ion Battery Electrolytes." *J. Electrochem. Soc.*, **168**, 080501 (2021).
17. G. A. Collins, H. Geaney, and K. M. Ryan, "Alternative Anodes for Low Temperature Lithium-Ion Batteries." *J. Mater. Chem. A*, **9**, 14172 (2021).
18. Q. Li, S. Jiao, L. Luo, M. S. Ding, J. Zheng, S. S. Cartmell, C.-M. Wang, K. Xu, J.-G. Zhang, and W. Xu, "Wide-Temperature Electrolytes for Lithium-Ion Batteries." *ACS Appl. Mater. Inter.*, **9**, 18826 (2017).
19. X. Ge and X. Wang, "Estimation of Freezing Point Depression, Boiling Point Elevation, and Vaporization Enthalpies of Electrolyte Solutions." *Ind. Eng. Chem. Res.*, **48**, 2229 (2009).
20. J. Newman and K. E. Thomas-Alyea, *Electrochemical Systems* (Wiley, Hoboken, New Jersey) (2004).
21. P. Debye and E. Huckel, "Zur Theorie der Elektrolyte." *Phys. Z*, **24**, 185 (1923).
22. G. Prentice, *Electrochemical Engineering Principles* (Prentice Hall, Upper Saddle River, New Jersey) (1991).
23. K. S. Pitzer, "Thermodynamics of Electrolytes. I. Theoretical Basis and General Equations." *J. Phys. Chem.*, **77**, 268 (1973).
24. K. S. Pitzer and G. Mayorga, "Thermodynamics of Electrolytes. II. Activity and Osmotic Coefficients for Strong Electrolytes with One or Both Ions Univalent." *J. Phys. Chem.*, **77**, 2300 (1973).
25. J. Barthel, R. Neueder, H. Poepke, and H. Wittmann, "Osmotic and Activity Coefficients of Nonaqueous Electrolyte Solutions. 1. Lithium Perchlorate in the Protic Solvents Methanol, Ethanol, and 2-Propanol." *J. Solution Chem.*, **27**, 1055 (1998).
26. J. Barthel, R. Neueder, H. Poepke, and H. Wittmann, "Osmotic Coefficients and Activity Coefficients of Nonaqueous Electrolyte Solutions. Part 2. Lithium Perchlorate in the Aprotic Solvents Acetone, Acetonitrile, Dimethoxyethane, and Dimethylcarbonate." *J. Solution Chem.*, **28**, 489 (1999).
27. N. Xin, Y. Sun, C. J. Radke, and J. M. Prausnitz, "Osmotic and activity coefficients for five lithium salts in three non-aqueous solvents." *J. Chem. Thermodyn.*, **132**, 83 (2019), Publisher: Elsevier.
28. L. Blum, "Mean Spherical Model for Asymmetric Electrolytes: I. Method of Solution." *Mol. Phys.*, **30**, 1529 (1975).
29. Y. Marcus and G. Hefter, "Ion Pairing." *Chem. Rev.*, **106**, 4585 (2006).
30. M. Born, "Volumen und Hydratationswärme der Ionen." *Zeitschrift für Physik*, **1**, 45 (1920).
31. P. Atkins and J. De Paula, *Physical Chemistry* (W.H. Freeman, New York, NY) 8th ed. (2006).
32. J. N. Israelachvili, *Intermolecular and Surface Forces* (Academic, New York, NY) (2011).
33. L. De Maeyer and G. Kessling, "Ion-Solvation and Ion-Pair Equilibria in Electrolyte Solutions." *J. Mol. Liq.*, **67**, 193 (1995).
34. Y. Marcus, "Ionic Radii in Aqueous Solutions." *Chem. Rev.*, **88**, 1475 (1988).
35. R. Buchner, G. T. Hefter, and P. M. May, "Dielectric Relaxation of Aqueous NaCl Solutions." *J. Phys. Chem. A*, **103**, 1 (1999).
36. S. Schlumpberger and M. Z. Bazant, *Simple Theory of Ionic Activity in Concentrated Electrolytes* (2017), arXiv:1709.03106.
37. P. Eberspächer, E. Wismeth, R. Buchner, and J. Barthel, "Ion Association of Alkaline and Alkaline-earth Metal Perchlorates in Acetonitrile." *J. Mol. Liq.*, **129**, 3 (2006).
38. E. L. Guggenheim, "The Specific Thermodynamic Properties of Aqueous Solutions of Strong Electrolytes." *Philos. Mag.*, **19**, 588 (1935).
39. J. M. Barthel, H. Krienke, and W. Kunz, *Physical Chemistry of Electrolyte Solutions: Modern Aspects* (Springer , New York, NY) (1998).
40. B. Maribo-Mogensen, G. M. Kontogeorgis, and K. Thomsen, "Comparison of the Debye-Hückel and the Mean Spherical Approximation Theories for Electrolyte Solutions." *Ind. Eng. Chem. Res.*, **51**, 5353 (2012).
41. A. R. Crothers, C. J. Radke, and J. M. Prausnitz, "110th Anniversary : Theory of Activity Coefficients for Lithium Salts in Aqueous and Nonaqueous Solvents and in Solvent Mixtures." *Ind. Eng. Chem. Res.* , **58**, 18367 (2019).
42. K. L. Gering, "Prediction of Electrolyte Conductivity: Results from a Generalized Molecular Model Based on Ion Solvation and a Chemical Physics Framework." *Electrochim. Acta*, **225**, 175 (2017).
43. M. Delsignore, H. Farber, and S. Petrucci, "Ionic conductivity and Microwave Dielectric Relaxation of Lithium Hexafluoroarsenate ($LiAsF_6$) and Lithium Perchlorate ($LiClO_4$) in Dimethyl Carbonate." *J. Phys. Chem.*, **89**, 4968 (1985).
44. J.-P. Simonin, L. Blum, and P. Turq, "Real Ionic Solutions in the Mean Spherical Approximation. 1. Simple Salts in the Primitive Model." *J. Phys. Chem.*, **100**, 7704 (1996).
45. J.-P. Simonin, O. Bernard, and L. Blum, "Real Ionic Solutions in the Mean Spherical Approximation. 3. Osmotic and Activity Coefficients for Associating Electrolytes in the Primitive Model." *J. Phys. Chem. B*, **102**, 4411 (1998).
46. J. Self, K. D. Fong, and K. A. Persson, "Transport in Superconcentrated $LiPF_6$ and $LiBF_4$/Propylene Carbonate Electrolytes." *ACS Energy Lett.*, **4**, 2843 (2019).
47. J. R. Pliego and J. M. Riveros, "The Cluster-Continuum Model for the Calculation of the Solvation Free Energy of Ionic Species." *J. Phys. Chem. A*, **105**, 7241 (2001).
48. M. Ue, "Mobility and Ionic Association of Lithium Salts in a Propylene Carbonate-Ethyl Methyl Carbonate Mixed Solvent." *J. Electrochem. Soc.*, **142**, 2577 (1995).
49. R. Schmid, A. M. Miah, and V. N. Sapunov, "A New Table of the Thermodynamic Quantities of Ionic Hydration: Values and Some Applications (Enthalpy-Entropy Compensation and Born Radii)." *Phys. Chem. Chem. Phys.*, **2**, 97 (2000).
50. M. Ue, "Mobility and Ionic Associationof Lithium and Quaternary Ammonium Salts in Propylene Carbonate and/-Butyrolactone." *J. Electrochem. Soc.*, **141**, 3336 (1994).
51. J. Tomasi, B. Mennucci, and R. Cammi, "Quantum Mechanical Continuum Solvation Models." *Chem. Rev.*, **105**, 2999 (2005).
52. J. Self, K. D. Fong, E. R. Logan, and K. A. Persson, "Ion Association Constants for Lithium Ion Battery Electrolytes from First-Principles Quantum Chemistry." *J. Electrochem. Soc.*, **166**, A3554 (2019).
53. S. J. Cox, K. K. Mandadapu, and P. L. Geissler, "Quadrupole-Mediated Dielectric Response and the Charge-Asymmetric Solvation of Ions in Water." *J. Chem. Phys.*, **154**, 244502 (2021).
54. M. Nie, D. P. Abraham, D. M. Seo, Y. Chen, A. Bose, and B. L. Lucht, "Role of Solution Structure in Solid Electrolyte Interphase Formation on Graphite with $LiPF_6$ in Propylene Carbonate." *J. Phys. Chem. C*, **117**, 25381 (2013).
55. D. M. Seo, S. Reininger, M. Kutcher, K. Redmond, W. B. Euler, and B. L. Lucht, "Role of Mixed Solvation and Ion Pairing in the Solution Structure of Lithium Ion Battery Electrolytes." *J. Phys. Chem. C*, **119**, 14038 (2015).
56. X. Bogle, R. Vazquez, S. Greenbaum, A. v. W. Cresce, and K. Xu, "Understanding Li^+-Solvent Interaction in Nonaqueous Carbonate Electrolytes with ^{17}O NMR." *J. Phys. Chem. Lett.*, **4**, 1664 (2013).
57. K. Kondo, M. Sano, A. Hiwara, T. Omi, M. Fujita, A. Kuwae, M. Iida, K. Mogi, and H. Yokoyama, "Conductivity and Solvation of Li^+ Ions of $LiPF_6$ in Propylene Carbonate Solutions." *J. Phys. Chem. B*, **104**, 5040 (2000).
58. I. Skarmoutsos, V. Ponnuchamy, V. Vetere, and S. Mossa, "Li^+ Solvation in Pure, Binary, and Ternary Mixtures of Organic Carbonate Electrolytes." *J. Phys. Chem. C*, **119**, 4502 (2015).
59. O. Borodin, M. Olguin, P. Ganesh, P. R. C. Kent, J. L. Allen, and W. A. Henderson, "Competitive Lithium Solvation of Linear and Cyclic Carbonates from Quantum Chemistry." *Phys. Chem. Chem. Phys.*, **18**, 164 (2016).
60. S. Hwang, D.-H. Kim, J. H. Shin, J. E. Jang, K. H. Ahn, C. Lee, and H. Lee, "Ionic Conduction and Solution Structure in $LiPF_6$ and $LiBF_4$ Propylene Carbonate Electrolytes." *J. Phys. Chem. C*, **122**, 19438 (2018).
61. R. Payne and I. E. Theodorou, "Dielectric Properties and Relaxation in Ethylene Carbonate and Propylene Carbonate." *J. Phys. Chem.*, **76**, 2892 (1972).
62. M. J. Frisch, G. W. Trucks, and H. B. Schlegel et al., Gaussian 16 Rev A.03, Gaussian, Inc., Wallingford CT (2016).
63. J.-D. Chai and M. Head-Gordon, "Long-range Corrected Hybrid Density Functionals with Damped Atom-Atom Dispersion Corrections." *Phys. Chem. Chem. Phys.*, **10**, 6615 (2008).
64. J. Self, N. T. Hahn, K. D. Fong, S. A. McClary, K. R. Zavadil, and K. A. Persson, "Ion Pairing and Redissociaton in Low-Permittivity Electrolytes for Multivalent Battery Applications." *J. Phys. Chem. Lett.*, **11**, 2046 (2020).
65. E. Cancès, B. Mennucci, and J. Tomasi, "A New Integral Equation Formalism for the Polarizable Continuum Model: Theoretical Background and Applications to Isotropic and Anisotropic Dielectrics." *J. Chem. Phys.*, **107**, 3032 (1997).
66. R. F. Ribeiro, A. V. Marenich, C. J. Cramer, and D. G. Truhlar, "Use of Solution-Phase Vibrational Frequencies in Continuum Models for the Free Energy of Solvation." *The Journal of Physical Chemistry B*, **115**, 14556 (2011).
67. G. Luchini, J. V. Alegre-Requena, I. Funes-Ardoiz, and R. S. Paton, "GoodVibes: Automated Thermochemistry for Heterogeneous Computational Chemistry Data." *F1000Research*, **9**, 291 (2020).
68. J. Self, B. M. Wood, N. N. Rajput, and K. A. Persson, "The Interplay between Salt Association and the Dielectric Properties of Low Permittivity Electrolytes: The Case of $LiPF_6$ and $LiAsF_6$ in Dimethyl Carbonate." *J. Phys. Chem. C*, **122**, 1990 (2018).
69. N. T. Hahn, J. Self, T. J. Seguin, D. M. Driscoll, M. A. Rodriguez, M. Balasubramanian, K. A. Persson, and K. R. Zavadil, "The Critical Role of Configurational Flexibility in Facilitating Reversible Reactive Metal Deposition from Borohydride Solutions." *J. Mater. Chem. A*, **8**, 7235 (2020).
70. L. Martínez, R. Andrade, E. G. Birgin, and J. M. Martínez, "PACKMOL: A Package for Building Initial Configurations for Molecular Dynamics Simulations." *J. Comput. Chem.*, **30**, 2157 (2009).
71. M. J. Abraham, T. Murtola, R. Schulz, S. Páll, J. C. Smith, B. Hess, and E. Lindahl, "GROMACS: High Performance Molecular Simulations Through Multi-Level Parallelism from Laptops to Supercomputers." *SoftwareX*, **1–2**, 19 (2015).
72. H. J. C. Berendsen, J. P. M. Postma, W. F. van Gunsteren, A. DiNola, and J. R. Haak, "Molecular Dynamics with Coupling to an External Bath." *J. Chem. Phys.*, **81**, 3684 (1984).
73. G. Bussi, D. Donadio, and M. Parrinello, "Canonical Sampling Through Velocity Rescaling." *J. Chem. Phys.*, **126**, 014101 (2007).
74. J.-C. Soetens, C. Millot, and B. Maigret, "Molecular Dynamics Simulation of LiBF4 in Ethylene Carbonate, Propylene Carbonate and Dimethyl Carbonate solvents." *J. Phys. Chem. A*, **102**, 1055–1061 (1998).
75. MacroModel, Schrödinger, LLC, New York NY (2019).
76. W. L. Jorgensen, "Free Energy Calculations: a Breakthrough for Modeling Organic Chemistry in Solution." *Acc. Chem. Res.*, **22**, 184 (1989).
77. W. L. Jorgensen, D. S. Maxwell, and J. Tirado-Rives, "Development and Testing of the OPLS All-Atom Force Field on Conformational Energetics and Properties of Organic Liquids." *J. Am. Chem. Soc.*, **118**, 11225 (1996).
78. B. Doherty, X. Zhong, S. Gathiaka, B. Li, and O. Acevedo, "Revisiting OPLS Force Field Parameters for Ionic Liquid Simulations." *J. Chem. Theory Comput.*, **13**, 6131 (2017).

79. J. N. Canongia Lopes, J. Deschamps, and A. A. H. Pádua, "Modeling Ionic Liquids Using a Systematic All-Atom Force Field." *J. Phys. Chem. B*, **108**, 2038 (2004).
80. S. Ding, K. Xu, S. Zhang, T. Jow, K. Amine, and G. Henriksen, "Diminution of Supercooling of Electrolytes by Carbon Particles." *J. Electrochem. Soc.*, **146**, 3974 (1999).
81. S. Petrucci, M. C. Masiker, and E. M. Eyring, "The Possible Presence of Triple Ions in Electrolyte Solutions of Low Dielectric Permittivity." *J. Solution Chem.*, **37**, 1031 (2008).
82. H. Lee, S. Hwang, M. Kim, K. Kwak, J. Lee, Y.-K. Han, and H. Lee, "Why Does Dimethyl Carbonate Dissociate Li Salt Better Than Other Linear Carbonates? Critical Role of Polar Conformers.." *J. Phys. Chem. Lett.*, **11**, 10382 (2020).
83. L. Doucey, M. Revault, A. Lautié, A. Chaussé, and R. Messina, "A Study of the Li/Li^+ Couple in DMC and PC Solvents: Part I: Characterization of LiAsF6/DMC and $LiAsF_6$/PC Solutions." *Electrochim. Acta*, **44**, 2371 (1999).
84. S. Stewart and J. Newman, "Measuring the Salt Activity Coefficient in Lithium-Battery Electrolytes." *J. Electrochem. Soc.*, **155**, A458 (2008).
85. M. S. Ding, "Electrolytic Conductivity and Glass Transition Temperature as Functions of Salt Content, Solvent Composition, or Temperature for $LiPF_6$ in Propylene Carbonate + Diethyl Carbonate." *J. Chem. Eng. Data*, **48**, 519 (2003).
86. G. Szklarz, K. Adrjanowicz, and M. Paluch, "Cooling-Rate vs Compression-Rate Dependence of the Crystallization in the Glass-Forming Liquid, Propylene Carbonate." *Cryst. Growth Des.*, **18**, 2538 (2018).